

Covalency in transition metal oxides within all-electron Dynamical Mean Field Theory

Kristjan Haule,* Turan Birol, and Gabriel Kotliar

Department of Physics and Astronomy, Rutgers University, Piscataway, NJ 08854.

(Dated: August 19, 2014)

A combination of dynamical mean field theory and density functional theory, as implemented in Phys. Rev. B 81, 195107 (2010), is applied to both the early and late transition metal oxides. For a fixed value of the local Coulomb repulsion, without fine tuning, we obtain the main features of these series, such as the metallic character of SrVO₃ and the insulating gaps of LaVO₃, LaTiO₃ and La₂CO₄ which are in good agreement with experiment. This study highlights the importance of local physics and high energy hybridization in the screening of the Hubbard interaction and how different low energy behaviors can emerge from the a unified treatment of the transition metal series.

I. INTRODUCTION

The quantum mechanical description of electrons in solids – the band theory¹⁻³ – offered a straightforward account for distinctions between insulators and metals. Fermi liquid theory⁴ has elucidated why interactions between 10^{23} cm⁻³ electrons in simple metals can be readily neglected, thus validating inferences of free electron models. It came as a considerable surprise in late 30s when crystals with incomplete *d* bands were found insulating⁵. The term "Mott insulator" was later coined to identify a class of solids violating the above fundamental expectations of band theory⁶. Peierls and Mott stated⁷ that "a rather drastic modification of the present electron theory of metals would be necessary in order to take these facts into account" and proposed that such a modification must include Coulomb interactions between the electrons. Study of correlations in solids, which are responsible for such a dramatic increase of resistivity in Mott insulators, remains in the forefront of contemporary condensed matter physics^{8,9}, and it was later found in many other materials, such as *d* and *f*-electron inter-metallic compounds, as well as a number of π -electron organic conductors.

The theory became predictive with the invention of the Density Functional Theory (DFT)¹⁰. Within the Kohn-Sham framework, the computation of the density of the solid is reduced to a tractable problem of non-interacting electrons moving in an effective potential. The implementation of DFT within the local density approximation (LDA) and generalized gradient approximations (GGA) in 1970s, and the increase in computational power in the past decades made it possible to predict materials properties *ab initio*. In weakly correlated materials the computed Kohn-Sham spectra is a reasonable description of the electronic spectra. However, materials with strong correlations, and in particular Mott insulators, are not properly treated within these approximations.

It's long been recognized that electron correlations are mostly local in space – two widely separated electrons are unlikely to be significantly correlated. Within LDA, the Kohn-Sham potential in each point of space depends solely on the density at the same point, hence LDA is local for each point in 3D-space. However, in solids with

partially filled *d*-bands, the correlations are very strong between two electrons on the same transition metal ion, which is beyond the scope of LDA.

In 1990s the Dynamical Mean Field theory (DMFT)¹¹⁻¹⁴ was developed. This theory introduces non-locality in time, which is essential for description of paramagnetic Mott insulators. This theory is also a local theory, but it is local to a given site rather than a point in space. DMFT successfully predicted the Mott-transition in the Hubbard model¹⁵⁻¹⁷, as well as many other known features of correlated systems, such as the dynamical spectral weight transfer¹⁸, the existence of a Mott end-point, and the value of the critical exponents at this Mott end-point¹⁹. The cluster-DMFT studies²⁰ show that this properties are genuine to the frustrated Hubbard model.

Within DMFT, the functional that contains all local correlations is known exactly, and can be calculated by solving an appropriate quantum impurity model, but the computational cost when including many interacting degrees of freedom on a given site increases exponentially, while the hybridization with non-interacting states does not increase the computational cost significantly. At present, modern computers allow us to treat interactions exactly within a complete *d* shell of a transition metal ion or a complete *f* shell in an inter-metallic compound, while the rest of the states must be treated by a mean-field method. The most popular choice of such a mean-field method is DFT, hence the combination of the two methods, first proposed in 1997²¹, was named LDA+DMFT^{22,23}. The method became very successful as it could predict properties of an extraordinary number of correlated materials previously resisting detailed material specific predictions (for a review see 22,23). The electronic structure and unusual physical properties of many actinides²⁴⁻²⁶, lanthanides²⁷⁻³⁰, $3d$ ³¹⁻³⁵, $4d$ ^{36,37} and $5d$ ³⁸ transition metal compounds were explained using this approach.

In the early 2000s, the LDA+DMFT method was usually referring to the dynamical mean field calculation of a lattice model, namely the Hubbard model, where the hopping parameters were derived by a so-called down-folding procedure: The bands near the Fermi level were represented in terms of a small number of Wannier states³⁹, and the resulting Hubbard model was solved

by the DMFT method. The feedback of correlations to the electronic charge distribution, and hence the Kohn-Sham potential, was often neglected. Also, usually the minimum number of Wannier states were kept in the model, which made such model calculations conceptually simple, but less predictive, as the Coulomb repulsion for a low energy model is strongly screened by the degrees of freedom eliminated from the model, hence a material specific and model specific calculation of the interaction strength U was needed to make this method predictive. The constrained-RPA^{40,41} was invented for that purpose, and was quite successful when the correlations are applied in the narrow energy window.

An alternative route, which avoids construction of the low-energy model, was proposed by Savrasov & Kotliar⁴², in which the correction (self-energy) due to the correlations is added to the Kohn-Sham potential in a very limited region of the real space, such as the muffin-tin (MT) sphere of the correlated ion. In this approach, all degrees of freedom local to an ion are treated exactly, while the non-local correlations are treated in a mean-field way by DFT. No valence state is eliminated from the model! Kohn-Sham potential is computed on the self-consistent electronic charge. We call this methodology the all-electron method. The early implementation of this approach, together with electronic charge self-consistency, successfully predicted the phonon spectra of elemental plutonium²⁵, but the impurity solvers at that time were not adequate to address many other challenging problems in correlated solids. The DFT+DMFT method has rapidly matured over the last few years, as several charge self-consistent implementations in various electronic structure codes appeared⁴³⁻⁴⁸, some with integrated state of the art impurity solvers^{43,48}.

The most significant difference between the earlier and more modern implementations of the method is the degree of localization of the electronic orbitals, which interact with strong Coulomb interaction. In the early days, a set of Wannier orbitals spanning a narrow window around the Fermi level was typically treated by the DMFT. Since the non-local interactions and the non-local correlations are neglected in the DMFT approach, one expects that a more localized choice of orbitals leads to better results within single-site DMFT approximation. Hence newer implementations applied correlations to more localized states, and kept a larger number of itinerant states in the model. A real space projector to the spherical harmonics within a MT-sphere around the correlated ion $P_R(\mathbf{r}\mathbf{r}', lml'm') = Y_{lm}(\hat{\mathbf{r}})\delta_R(r-r')Y_{l'm'}^*(\hat{\mathbf{r}}')$ (where $\delta_R(r-r')$ is nonzero when $r < R$ and $r' < R$) is a good example of extremely localized orbitals, which hybridizes with a large number of Kohn-Sham states,

spanning a large energy window in band representation. Such a set of real-space orbitals is clearly more localized than the popular choice of maximally localized Wannier orbitals⁴⁹, which are constrained to faithfully represent some set of low energy bands.

Numerous successful predictions of this all-electron DFT+DMFT were published in the past decade nevertheless, its predictive power for transition metal oxides was questioned recently in Refs. 50,51. Namely, using Wannier functions for oxygen- p states and transition metal d states, the authors of Refs. 50,51 concluded that fine tuning of several parameters, including the double-counting and the interaction U is needed to describe the Mott insulating state in early and late transition metal oxides. Moreover, the $p-d$ model requires occupancy of the d orbitals to be close to unity for the Mott state, while DFT solution projected to the orbitals of their choice, predicts far larger occupancies, hence this discrepancy between DFT occupancies and the DMFT requirements lead them to suggest that the self-consistent DFT+DMFT can not describe the Mott insulating state without fine tuning the interaction U to be in the narrow range of 6 ± 1 eV and ad-hoc fine tuning of the double-counting to reproduce the experimentally observed $p-d$ splittings. This calls for a critical reexamination of the application of the LDA+DMFT to the $3d$ series.

Our methodology⁴³ was tested in numerous classes of materials, such as actinides^{52-56,59,61,63,65}, lanthanides^{26,43,68,70}, transition metal oxides^{57,60,64}, iron superconductors^{58,62,66,69}, and other transition metal compounds^{38,67}. However, results for early and late transition metal oxides with our methodology are not available in literature. It is therefore important to test our methodology in this class of materials, which have mostly been studied using downfolded LDA+DMFT implementations.

II. METHOD

In this work we perform DFT+DMFT calculations for a series of early transition metal oxides: SrVO₃, LaVO₃, LaTiO₃, and a cuprate parent compound La₂CuO₄; all the test cases which required fine tuning in Refs. 50,51. We show that no fine tuning or adjustable parameter is required in DFT+DMFT implementation of Ref. 43, and for a fixed value of on-site Coulomb repulsion $U = 10$ eV Mott gaps in all these compounds are in reasonable agreement with experiment.

The all-electron DFT+DMFT implementation⁴³ extremizes the following functional²²

$$\Gamma[\rho, V_{KS}, G_{loc}, \Sigma, V_{dc}, n_d] = -\text{Tr} \ln \left((i\omega + \mu + \nabla^2 - V_{KS})\delta(\mathbf{r} - \mathbf{r}') - \sum_{\tau LL'} P(\mathbf{r}\mathbf{r}', \tau LL')(\Sigma - V_{dc})_{L'L} \right) \quad (1)$$

$$- \int [V_{KS} - V_{ext}]\rho d^3r - \text{Tr}(\Sigma G_{loc}) + \text{Tr}(V_{dc}n_d) + \Phi_H[\rho] + \Phi_{xc}[\rho] + \Phi_{DMFT}[G_{loc}] - \Phi_{dc}[n_d]$$

of three pairs of conjugate variables. At the saddle point, ρ , V_{KS} are the electronic charge density, the Kohn-Sham potential, G_{loc} and Σ are the local Green's function and DMFT self-energy, V_{dc} is the double-counting potential, and n_d is the occupancy of the correlated orbital. $\Phi_H[\rho]$ and $\Phi_{xc}[\rho]$ are the Hartree and the exchange-correlation energy functionals, $\Phi_{DMFT}[G_{loc}]$ is the sum of all skeleton diagrams constructed from G_{loc} and local Coulomb repulsion \hat{U} . This summation is carried out by the impurity solver. The local Coulomb repulsion \hat{U} is parametrized with the Slater parametrization with $J_{Hunds} = 0.7$ eV, and, if not otherwise stated, $U = 10$ eV. The impurity model is solved by the continuous-time quantum Monte Carlo method^{71,72}.

V_{ext} is the external potential, containing the material specific information. $P(\mathbf{r}\mathbf{r}', \tau LL')$ is the projector to the local correlated orbital at atom τ with angular momentum indices L, L' . We use projector $P^2(\mathbf{r}\mathbf{r}', \tau LL')$ introduced in Ref. 43 with an energy window of ≈ 20 eV around the Fermi level. For the maximal locality of correlated states, this projector is implemented in real space and is nonzero only within the MT-sphere of the correlated ion. In section IV we test several different projectors, ranging from extremely localized to moderately delocalized, to understand the controversy in the literature regarding the DFT+DMFT results for the transition metal oxides. The vanadium and titanium t_{2g} states are treated dynamically, while the empty e_g states are treated by a static mean field. The copper ion with its almost full shell requires dynamic treatment of all five $3d$ orbitals.

For the double-counting correction, we used two methodologies: a) the fully-localized-limit (FLL) formula introduced in Ref. 73 is used in section IV to ensure that the results are robust and that the simplification used elsewhere does not change the results appreciably from this standard prescription. b) the method explained in Ref. 43 is used in most of this paper, where $\Phi_{dc}[n_d] = n_d V_{dc}$ and V_{dc} is also parameterized by the standard fully-localized-limit formula⁷³ $V_{dc} = U(n_d^0 - 1/2) - J/2(n_d^0 - 1)$, and n_d^0 is taken to be the nominal occupancy of the correlated ion. We name this method fixed-DC. In particular, for SrVO₃ with V⁴⁺ ion we take $n_d^0 = 1$, for LaVO₃ with V³⁺ ion $n_d^0 = 2$, for LaTiO₃ with Ti³⁺ ion $n_d^0 = 1$ and for La₂CuO₄ with Cu²⁺ ion $n_d^0 = 9$. This double-counting scheme has two virtues: i) it is numerically much more stable in the charge-self-consistent DFT+DMFT, as the noise from Monte-Carlo does not feed-back into impurity levels, and into large Hartree shifts. ii) the results

are more robust with respect to small changes in projector, linearization energies, etc. Both double-countings are equally justifiable on the phenomenological level. The determination of the exact double-counting is an open problem, but see recent progress in Ref. 96.

The double-counting b) ensures that at infinite U one recovers atomic physics at the nominal valence. For discussion's sake, let us set J_{Hunds} to zero. In the absence of any double-counting correction, the lower Hubbard band in the atomic limit is positioned at $\varepsilon_f + U(n_d^0 - 1)$, and the upper Hubbard band at $\varepsilon_f + Un_d^0$, where ε_f is the center of the correlated state at $U = 0$ (in DFT calculation). The center between the Hubbard bands is at $\varepsilon_f + U(n_d^0 - 1/2)$. To ensure that in the large U limit the center of the correlated states does not move from its DFT position, and that we recover the correct nominal occupancy, we must subtract from the dynamic self-energy the correction $U(n_d^0 - 1/2)$, which brings the center of the correlated state to its center in DFT. Hence a good choice for double counting correction (in the absence of Hunds coupling) is given by $U(n_d^0 - 1/2)$ with n_d^0 the nominal valence. In typical model calculations for the downfolded Hubbard model, such nominal valence is automatically enforced.

The DFT part of our code is based on the WIEN2k package⁷⁴. The exchange-correlation energy in DFT ($\Phi_{xc}[\rho]$) is evaluated using the PBE functional.⁷⁵ The DFT+DMFT calculations are fully self-consistent in the electronic charge density, chemical potential, and impurity levels. The temperature is set to 200K. The experimental crystal structures from Refs. 76, 77, 78 79 are used for SrVO₃, LaVO₃, LaTiO₃, La₂CuO₄, respectively. To obtain spectra on the real axis, maximum entropy method is used for analytical continuation of the self-energy.⁸⁰ Finally, the VESTA software is used at various points to visualize and study the crystal structures.⁸¹

III. RESULTS

Fig. 1 shows the DFT+DMFT total and projected $3d$ densities of states for the four test compounds. The photoemission measurements are also shown for comparison. Fig. 2 zooms the low energy part of the DOS to display the gap sizes. SrVO₃ is a mixed-valent ($n_d = 1.19$) metallic compound with oxygen states centered around -5 eV, a small shoulder corresponding to an incoherent excitation (Hubbard band) around -1.5 eV of mostly d character, and the quite broad quasiparticle peak at the Fermi level

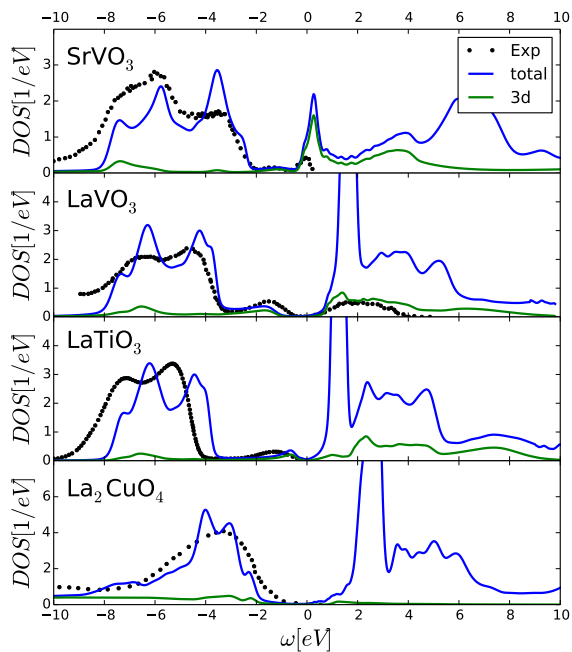


FIG. 1: The total DOS and its projection to the $3d$ ion for selected transition metal oxides. Experimental photoemission for SrVO_3 , LaVO_3 , LaTiO_3 , and La_2CuO_4 is plotted by black dots, and was digitized from Refs. 82, 83, 84, 85, respectively.

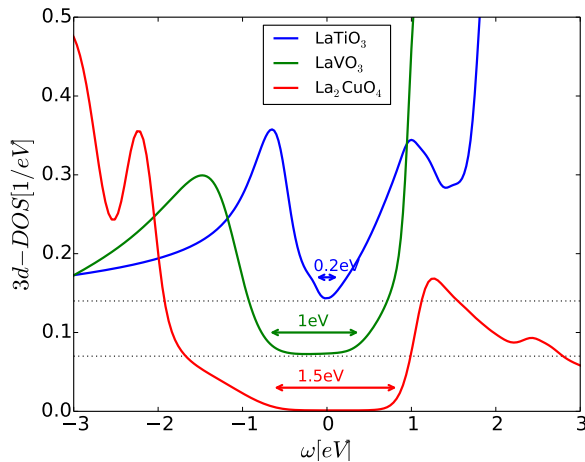


FIG. 2: Zoom-in of the low-energy DOS projected to the $3d$ orbitals for insulating compounds. For clarity, the curves were offset for $0.07/\text{eV}$. The arrows mark the experimental size of the gap.

with its bandwidth reduced from DFT for roughly a factor of 2. These are all in excellent agreement with the experiment^{82,86,94}. Previous LDA+DMFT calculations of Refs. 31,94, where only the t_{2g} states were treated in the model, gave very similar electronic spectra, hence results are very robust with respect to the choice of the

correlated orbital. Notice that the value of U depends on the choice of energy window. Calculations with an energy window, which include only the t_{2g} states, requires a value of $U \approx 5$ eV, as used in Ref. 31. For large energy window (20 eV used here) somewhat larger value of U is needed, however, results are reasonable for an extended range of U values between 6-10 eV.

LaVO_3 is a Mott-insulator with a gap size of approximately 1 eV (see Fig. 2), in agreement with experiment⁸³. The lower Hubbard band at -1.5 eV, has a considerably more admixture of oxygen- p than SrVO_3 , as noticed in Ref. 83. LaTiO_3 has a very small Mott gap around 0.2 eV, similar to the experimental gap⁸⁴. The Hubbard band is located at ≈ -0.8 eV, and the oxygen- p band edge is at -4 eV. Experimentally, the Hubbard band and oxygen band are located at somewhat lower energy than theoretically predicted. Our DFT+DMFT calculation does not shift the oxygen states appreciably from its DFT position. Finally, La_2CuO_4 is a wide-gap Mott insulator of charge-transfer nature, and has a gap size of the order of 1.5 eV and the position of the oxygen- p band around -3.5 eV. The oxygen position is well predicted by the theory, and also the gap value is in good agreement with experiment⁸. Overall agreement with the experiment is very satisfactory, considering that no tuning parameter is used in these calculations.

To show that the fine tuning of local Coulomb repulsion U , which gets screened by the valence states included in our DMFT calculations, is not needed to get reasonable agreement with experiment, we show below calculations for several values of U . We also display how valence changes with the increasing correlation strength U , and as expected, we show that an infinite U would lead to integer valence. Notice that the DFT+DMFT valence in the actinides⁵⁴ agrees with the experiment better than the LDA valence.

Fig. 3 shows the dependence of DOS in SrVO_3 on the local Coulomb repulsion U . In the plot we also show the occupancy of the $V-t_{2g}$ states as well as the photoemission spectra of thin film⁸². The $U = 0$ results correspond to the GGA calculation. The oxygen- p bands move to a slightly (< 0.5 eV) lower energy at $U = 6$ eV while they progressively move back to its DFT location at larger U . The quasiparticle peak slightly narrows with increasing U , but the Mott gap does not open even for very large U beyond 12 eV (not shown in the figure). Notice that this is inconsistent with the universal phase diagram in Fig. 2 of Ref. 51 since $n = 1.2$ falls deep inside the insulating regime for d^1 systems in that phase diagram. The lower Hubbard band, located between the quasiparticle peak and oxygen bands, appears at $U = 8$ eV and becomes even more pronounced at $U = 10$ eV. The system is very mixed-valent (non-integer occupancy) in GGA, but it becomes less mixed-valent with increasing U . As expected, increasing correlation strength typically reduces mixed-valency. As is clear from Fig. 3, results are not very sensitive to the strength of the Coulomb repulsion, and any value of U between 6-12 eV gives reasonable

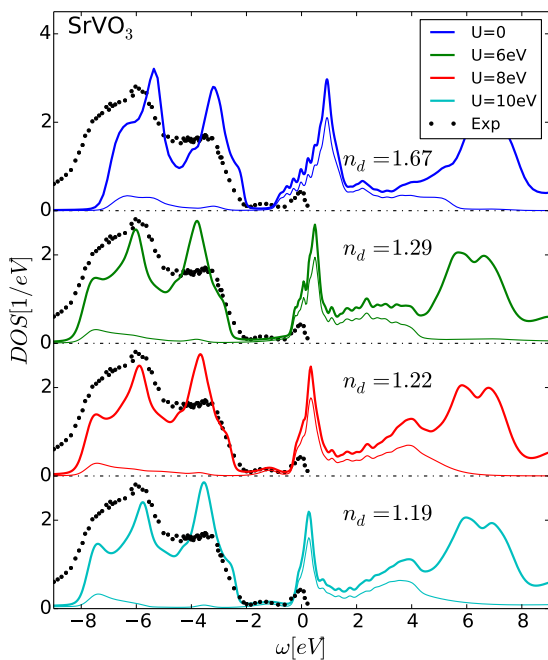


FIG. 3: The dependence of the electronic structure of SrVO₃ on the value of the local Coulomb repulsion U in this all-electron calculation. The text displays the valence of V^{4+} ion. The thick-line presents the total DOS and the thin-line its projection to the $3d$ -ion subset. For clarity, the different electronic structures are offset for 3eV .

agreement with experiment. The low energy t_{2g} spectra is in good agreement with earlier DMFT calculation of Ref. 31, which included only the t_{2g} states.

Fig. 4 displays DOS for LaVO₃ for a range of U values. In GGA, the t_{2g} states cross the Fermi level, while the oxygen- p bands are below -3.5eV and the La- f bands are just above the E_F . For the correlation strength of 4eV , LaVO₃ is still metallic, although the quasiparticle peak becomes extremely narrow, while the valence does not change appreciably from its GGA value. Larger $U = 6\text{eV}$ opens the Mott gap, (the critical U is approximately 5eV) and an incoherent shoulder appears around -1eV , and mixed-valency is reduced. Finally at $U = 10\text{eV}$ the Mott gap is of the order of 1eV and the position of the incoherent shoulder is at -1.5eV in good agreement with experiment⁸³. The partial occupancies of the t_{2g} orbitals at $U = 10\text{eV}$ are $n_{i2g}^1 = 0.56$, $n_{i2g}^2 = 0.76$, and $n_{i2g}^3 = 0.76$, hence the orbital fluctuations are strong due to the important role of Hund's coupling, which prevents orbital polarization. This is all in good agreement with earlier DMFT calculation of Ref. 33, which considered only the low energy t_{2g} degrees of freedom. Notice that the oxygen- p bands do not shift appreciably with increasing U and their position is well determined by DFT, in strong contrast to the calculations in Ref. 50, where the oxygen- p bands move substantially for a small change in U .

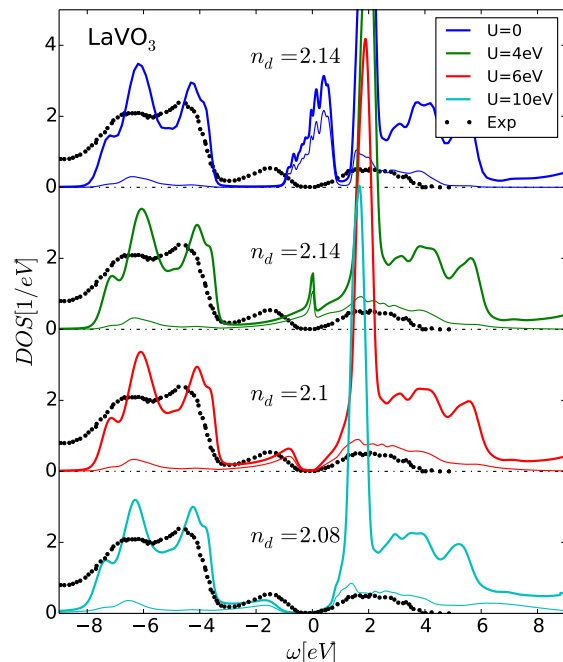


FIG. 4: The electronic structure of LaVO₃ for different values of the local Coulomb repulsion U . We also display the valence of V^{3+} ion.

In LaTiO₃, displayed in Fig. 5, the oxygen- p bands start around -4eV and a very sharp La- f state appears just above the Fermi level at 1eV . The position of this level is very sensitive to the rotation angle of the oxygen octahedra, and a larger rotation angle, which is obtained by the GGA-optimization of the structure, shifts the level up by 0.5eV compared to experimentally determined crystal structure⁷⁸ used here. This can be explained by the fact that octahedral rotations change the coordination of the A-site cation (La) drastically.⁸⁷ It is due to screening by this sharp La- f state that the Mott gap does not open for $U = 8\text{eV}$ and is very small ($\approx 0.2\text{eV}$) at $U = 10\text{eV}$.

The orbital polarization is also very sensitive to the octahedral rotation, as pointed out in Ref. 31. For the structure of Ref. 78, the orbital polarization is modest in our calculations ($n_{i2g}^1 \approx 0.67$, $n_{i2g}^2 \approx 0.20$, $n_{i2g}^3 \approx 0.20$) but for only slightly larger rotation, as measured in Ref. 88, the polarization is almost complete ($n_{i2g}^1 \approx 0.93$, $n_{i2g}^2 \approx 0.06$, $n_{i2g}^3 \approx 0.08$).

Due to the substantial hybridization of the t_{2g} states with the La- f states very near the Fermi energy (see Fig. 8), the screening is much stronger than it would be in the absence of this La- f level. Models which remove the La- f states from consideration would hence need substantially reduced interaction U to reproduce the experimentally observed Mott gap⁸⁴. Indeed, our results clearly disagree with the phase diagram of Ref. 51, which leads us to believe that the $U-n_d$ phase diagram is more mate-

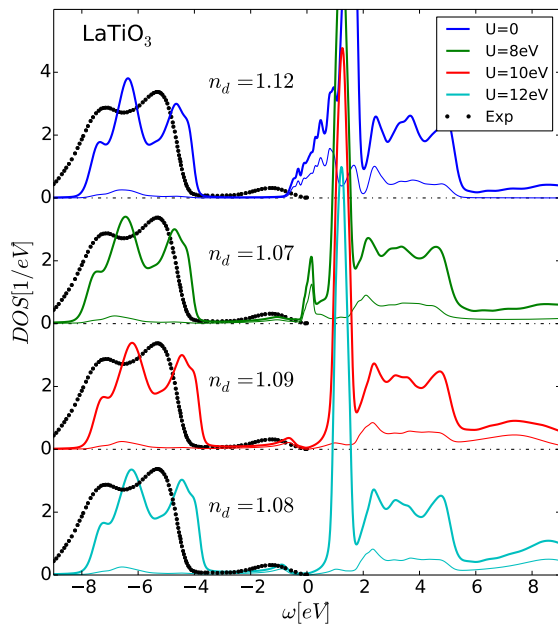


FIG. 5: The electronic structure of LaTiO_3 for different values of the local Coulomb repulsion U . We also display the valence of Ti^{3+} ion.

rial specific, and also depends on presence of other states that can screen the interaction. To open a Mott gap, a near integer occupancy is needed, but the critical value of U and n_d can be quite material specific. Notice that the double counting is also proportional to the Coulomb interaction U , hence in the large U limit, the upper and lower Hubbard bands are pushed to positive and negative infinity respectively; always resulting in an integer occupancy. We also display photoemission measurements for $\text{La}_{1-x}\text{Sr}_x\text{TiO}_{3+y}$ with $x + y = 0.04$ from Ref. 84. The oxygen- p bands' position is somewhat different than in experiment. However, this disagreement between DFT and experiment might partially be attributed to slightly different chemical composition of the crystal. The local correlations on Ti do not improve the position of O- p state.

Fig. 6 shows the DOS for La_2CuO_4 , a late transition metal oxide, and the parent compound of cuprate superconductors. Within GGA ($U = 0$), the e_g states cross the Fermi level and the t_{2g} states start at -1 eV and strongly overlap with oxygen, which starts at -2 eV. The sharp peak at 2.5 eV is due to the La- f states. The screening by La- f states in cuprates is much weaker than in LaTiO_3 , as the hybridization function, displayed in Fig. 8, has only a very weak peak at higher energy (2.4 eV) which couples primarily to t_{2g} states, but not to low energy $x^2 - y^2$ orbital. Once again, the oxygen- p states and the La- f states do not move appreciably with increasing correlation strength. The Mott gap opens around $U = 8$ eV. As in the model Hamiltonian studies within single site DMFT, once the insulating phase is reached¹⁵, the gap

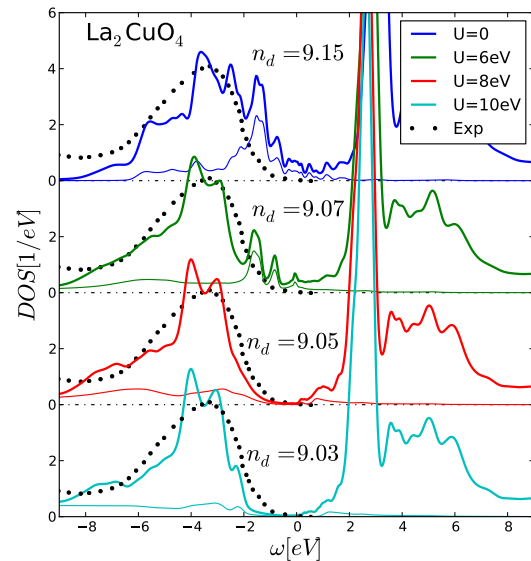


FIG. 6: The electronic structure of La_2CuO_4 for different values of the local Coulomb repulsion U . We also display the valence of Cu^{2+} ion.

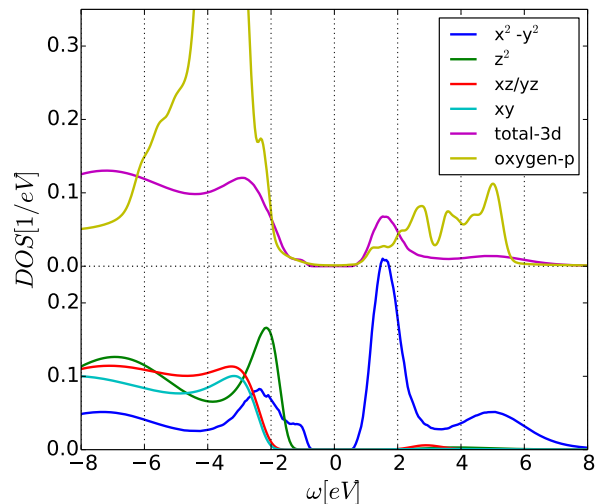


FIG. 7: Orbitally resolved DOS for La_2CuO_4 at $U = 10$ eV. The total-3d and total oxygen- p DOS is offset for 0.25/eV.

opens discontinuously, and is of the order of 1 eV. At $U = 10$ eV, it is approximately 1.5 eV, in agreement with the experiment⁸. The oxygen bands' position is also in a good agreement with the experiment⁸⁵, centered at -3.5 eV. Fig. 7 resolves DOS in orbital space. Clearly, the $x^2 - y^2$ orbital is half-filled, and in the interval between -1 eV and -2 eV the amount of total-3d states and oxygen states is almost exactly equal. This is the region of the Zhang-Rice singlet. The z^2 orbital is sharply peaked slightly below -2 eV, and the t_{2g} states start at -3 eV.

A main finding of this paper is that the all-electron

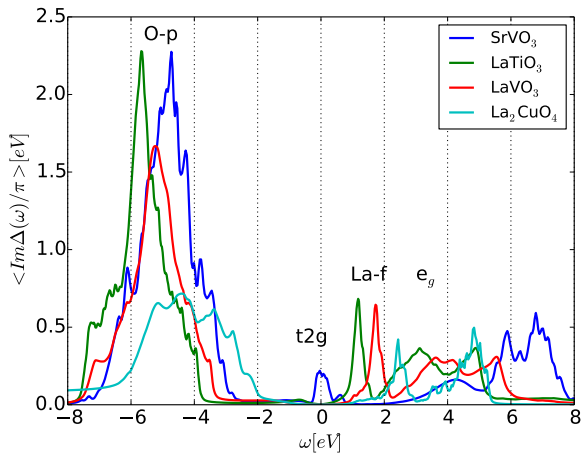


FIG. 8: The imaginary part of the impurity hybridization function for various materials at $U = 10$ eV. We also display what is the dominant source of various peaks in the hybridization function.

treatment with a large energy window requires a much larger value of U than the corresponding LDA+DMFT study with the small energy window, which keeps the t_{2g} (or e_g) states only. The bare Coulomb repulsion U of a model where all valence states are kept in the model is screened only by the degrees of freedom eliminated from the model, which are mostly core and semicore states, resulting in a much larger on-site Coulomb repulsion U in this treatment, but also more universal U across similar compounds. The screening from model- U down to the fully screened interaction W is achieved here by the impurity solver (see related discussion in the context of the model in Ref.95).

On the one particle level, it is best demonstrated by the impurity hybridization function, which contains signatures of all the valence states in the solid that screen the local degrees of freedom. We show in Fig. 8 the average hybridization function (average over orbitals) for an electron on transition metal site in different compounds. We can understand qualitatively the influence of the window on the characteristic scale of the impurity model from the following argument. The Kondo scale should not depend on the energy window chosen in the calculation. The Kondo scale is a function of U and impurity hybridization $T_k \approx \exp(-\text{const} * U / \langle \text{Im}\Delta \rangle_0)$, where $\langle \text{Im}\Delta \rangle_0$ is some weighted average of the displayed hybridization function, with larger weight given to the low energy. When only the t_{2g} states in early transition metal compounds are kept in the model, U has to be small, because the hybridization function is nonzero only within the narrow region around E_F , and its average value is below 0.2 eV. When oxygen- p states are added, $\text{Im}\Delta$ increases tremendously in the interval -7 eV to -3 eV, and so does the weighted average $\langle \text{Im}\Delta \rangle_0$, hence U must increase to keep low energy scale intact. It is also clear from Fig. 8 that

the La- f states screen the Coulomb repulsion rather well, since they are located very near the Fermi level; hence elimination of La- f states from the model would need to be compensated by a very material specific U . Finally, some extra screening is also coming from e_g states above the Fermi level, and since their position is very material dependent, their elimination requires further tuning of U . However, when all these states are kept in the model, the large part of the screening is already contained in the model, and hence the all-electron U is rather large and more universal.

IV. DISCUSSION AND COMPARISON TO OTHER STUDIES

To assess the robustness of our results, we also tested the widely used fully localized limit (FLL) double counting of Ref. 73, namely $V_{dc} = U(n_d - 1/2) - J/2(n_d - 1)$, where n_d in the formula is computed self-consistently. We note that this makes charge self-consistency convergence a bit more challenging, but the results for the transition metal insulators studies here, are almost identical to those presented above for fixed double counting.

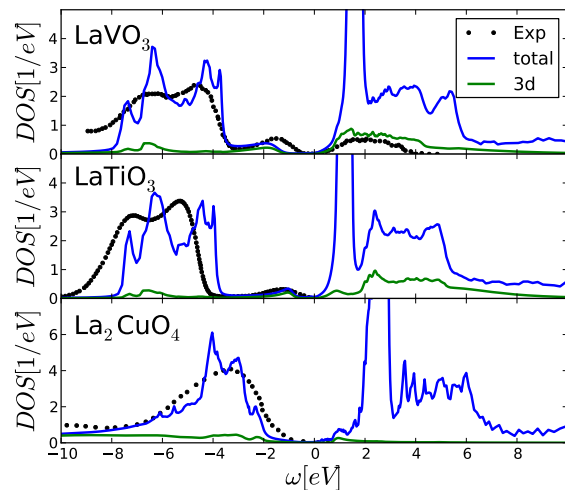


FIG. 9: The total DOS and its projection to the 3d ion within DFT+DMFT for insulating transition metal oxides, computed using standard fully localized limit double counting and fixed $U = 10$ eV and $J_{Hunds} = 0.7$ eV. Experimental photoemission is the same as in Fig. 1.

In Fig. 9 we plot the spectral functions of all four insulators but here computed using standard FLL double-counting. Comparison with Fig. 1 shows that the differences between the two double-countings are extremely small and unimportant in these cases. This is not surprising given the converged DFT+DMFT occupancy of the correlated d orbitals. In Table I we list the 3d occupancies for the calculations presented in Fig. 1 (de-

$n_d(\text{DFT} + \text{DMFT})$	fixed-DC CSC	FLL-DC CSC	FLL-DC non-CSC
La_2CuO_4 ($R_{MT} = 1.88$)	9.031	9.042	9.049
LaVO_3 ($R_{MT} = 1.97$)	2.075	2.098	2.093
LaTiO_3 ($R_{MT} = 2.01$)	1.093	1.131	1.133

TABLE I: The occupancy of the correlated $3d$ orbitals within DFT+DMFT calculation for insulating transition metal oxides. The first row is for double-counting introduced in section II (fixed-DC) and full charge self-consistent calculation (CSC). The second row stands for fully localized limit double-counting (FLL-DC) and charge self-consistency (CSS). The last column shows n_d for FLL-DC without charge self-consistency (non-CSS).

nominated by *fixed-DC*) and for the standard FLL double counting (denominated *FLL-DC*). Note that for the early transition metal oxides we count t_{2g} charge here, since correlations are applied to t_{2g} set of orbitals. For La_2CuO_4 , we list total $3d$ occupancy, since the correlations are applied to all $3d$ electrons. We also tested if charge self-consistency is important for insulating nature of these compounds. The charge-self consistent and non-charge self-consistent calculation is denoted by CSS and non-CSS in Table I. The differences in occupancies are insignificant. The double-counting used above (fixed-DC) makes the insulating state slightly more robust, since n_d is closest to nominal valence (of the order of 0.02 electron less than FLL-DC), the alternative FLL double-counting slightly increases mixed valency, while the charge-self consistency has very small effect (of the order of 0.005) in these transition metal oxides.

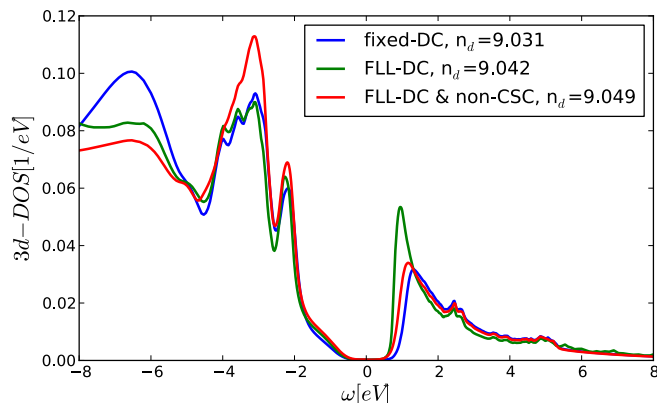


FIG. 10: The $3d$ density of states within DFT+DMFT for La_2CuO_4 using the three different methodologies explained in Table I.

In Fig. 10 we show the $3d$ -DOS for La_2CuO_4 in the three types of calculations listed in table I. There are some minor differences in the spectra distribution, and as expected from slightly larger n_d in FLL-DC case, the gap gets slightly smaller, but overall these differences are very small.

The above results appear to contradict conclusions of Ref. 50,51, in which the authors assert that $3d$ occupancy of LDA+DMFT calculations are consistently too large to allow Mott insulating state. The authors then proposed to adjust the double-counting energy to allow the opening of the Mott gap within their implementation of LDA+DMFT. They traced the problem to the d -occupancy being way too large even on the DFT level ($U = 0$). To define the d occupancy, they constructed the maximally localized Wannier orbitals with transition metal $3d$ and oxygen $2p$ orbitals included in the model, and excluding all the rest. In such a model, they noticed that the $3d$ occupancy in La_2CuO_4 is around $n_d \approx 9.45$, in LaVO_3 and in LaTiO_3 is around $n_{t_{2g}} \approx 2.55$, and $n_{t_{2g}} \approx 1.45$, respectively. These numbers are clearly larger than numbers obtained by our method at $U = 0$ in Figs. 4, 5, and 6, hence their work revealed difficulties with the formulation and implementation of DFT+DMFT when Wannier basis is not sufficiently localized.

To understand the difference, we implemented a flexible real space projectors, which generalize atomic like projectors introduced in Ref. 43, but can be extended into interstitial region or made very localized inside MT-sphere. The form of such a projector in real space is

$$P(l, m, lm', \mathbf{r}\mathbf{r}') = Y_{lm}(\hat{\mathbf{r}})\phi_l(r)\phi_l(r')Y_{lm'}(\hat{\mathbf{r}}') \quad (2)$$

In the above calculations, the projector was constructed from $\phi_l(r)$, which is a solution of the Dirac equation inside the muffin-tin sphere, and is zero outside the sphere. In the actual implementation of Ref. 43, we also added the small contribution coming from the energy derivative of the radial wave function, which turns out not to be important in these cases. Here we allow $\phi_l(r)$ to be any radial wave function constructed from solution of the Dirac equation $u_l(r, E_\nu)$ with E_ν positioned at the center of the band, its first ($du_l(r, E_\nu)/dE_\nu \equiv \dot{u}_l$) and second derivative ($d^2u_l(r, E_\nu)/d^2E_\nu = \ddot{u}_l$). To gain an insight into the precise definition of the n_d occupancy, we projected the Kohn-Sham solution to the variety of projectors, spanning the range of very localized to moderately delocalized, using a linear combination of above defined functions: $\phi(r) = au_l(r) + b\dot{u}_l(r) + c\ddot{u}_l(r)$. First we choose a very localized function $\phi(r)$ entirely contained in the MT-sphere and vanishing at the sphere with vanishing derivative. We name the corresponding projector *Proj(1)* in Fig. 11. (Here the MT-spheres are chosen in such a way that the spheres of neighboring atoms touch). Notice that such combination of u_l , \dot{u}_l and \ddot{u}_l roughly corresponds to choosing the linearization energy at the bottom of the corresponding bands.

The second projector *Proj(2)* takes u_l only (i.e., sets b and c to zero, hence linearization energy is taken at the middle of the corresponding band), but it truncates the radial function at the MT-sphere. This projector is very similar to what is used in chapter III of this paper. (The precise definition, which includes the correction due to \dot{u} can be found in Ref.43.) Finally, we extended the projec-

tor to the interstitial region with projector $Proj(3)$. Inside MT-sphere, we choose u_l as in $Proj(2)$, and outside we choose linear combination of u_l , \dot{u}_l and \ddot{u}_l such that the function vanishes at the nearest neighbor oxygen, and is continuous differentiable across the MT-sphere. When projecting the Kohn-Sham solution to the function $\phi(r)$ beyond the MT-sphere of the $3d$ -ion ($r > R_{mt}$), we project to the plane-wave envelop functions only, to excluded the density concentrated inside the oxygen MT-spheres, which should not be counted as transition metal charge. We always normalize the projector, to exclude the trivial effect of volume increase.

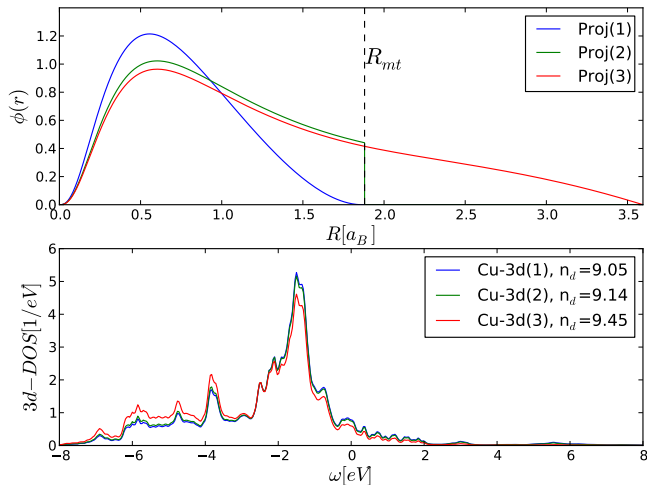


FIG. 11: The radial dependence of the function $\phi(r)$, which defines the projector to the correlated $3d$ set of orbitals. Three different projectors ($Proj(1)$, $Proj(2)$ and $Proj(3)$) are defined in the upper panel. Lower panel shows the density of states within LDA for La_2CuO_4 using the three different projectors defined in the upper panel.

In Fig. 11 we show the radial functions $\phi(r)$ for these three projectors in the case of La_2CuO_4 , together with the DFT projected density of states (more precisely $-\text{Im}(G_d(\omega))$). As is clear from the figure, the more delocalized projector has substantially more weight in the region between -7 to -4 eV, in the energy where oxygen is concentrated, while the localized projectors have more weight at the upper edge of the DOS and less concentrated around oxygen. The net result is a different occupancy n_d . In table II we list the DFT occupancies obtained by projecting to these three projectors and for all compounds studied here. We again project to t_{2g} states for early transition metal oxides, and to eg and t_{2g} states in La_2CuO_4 , because these are the states which are correlated in the DMFT calculations. For La_2CuO_4 , we notice that the two localized projectors ($Proj(1)$ and $Proj(2)$) both have occupancy close to nominal d^9 , and that the projector $Proj(2)$ has slightly more charge (1% increase) than the most localized $Proj(1)$. As shown by direct DFT+DMFT calculation above, $Proj(2)$ gives the Mott insulating state in La_2CuO_4 irrespective of small details

$n_d(DFT)$	Proj(1)	Proj(2)	Proj(3)
La_2CuO_4	9.040	9.131	9.450
LaVO_3	2.096	2.193	2.872
LaTiO_3	1.097	1.195	1.960
SrVO_3	1.692	1.815	2.567

TABLE II: The occupancy of the $3d$ orbitals using DFT (at $U = 0$) for the three projectors shown in Fig. 11. The MT-spheres are listed in Table I.

in double-counting (fixed-DC or FLL-DC) or charge-self-consistency. On the other hand, $Proj(3)$, which extends beyond the MT-boundary, contains some of the charge that should have been assigned to other itinerant states. As a result, it gives occupancy $n_d = 9.45$, almost identical to the charge on the Wannier orbitals of Ref. 50. Since construction of Wannier orbitals inevitable results in some fraction of electrons being delocalized beyond the MT-boundary, it is not surprising that the $3d$ occupancy is similar to our more delocalized projector. Namely, maximally localized Wannier orbitals need to faithfully represent a set of low energy bands, hence their localization is constrained to this condition. We verified that DFT+DMFT solution using $Proj(3)$ and FLL-DC results in metallic state, similar to finding of Ref. 50.

For the insulating early transition metal oxides, the t_{2g} occupancies of both localized projectors $Proj(1)$ and $Proj(2)$ are again quite close to nominal valence, namely d^1 for LaTiO_3 and d^2 for LaVO_3 . On the other hand, the delocalized projector $Proj(3)$ results in much larger n_d , even larger than reported in Ref. 50,51. Hence, Wannier orbitals in Ref. 51 are more localized than our $Proj(3)$, but less than $Proj(2)$ or $Proj(1)$. We verified that increasing localization of the projector always results in increased n_d occupancy. The Mott state within DFT+DMFT is again very robust using $Proj(1)$ and $Proj(2)$, but not when $Proj(3)$ is used. Finally, the $3d$ occupancy in SrVO_3 is quite far from nominal d^1 valence even when using very localized projectors, and hence this mixed-valency results in metallic state even for very large values of local Coulomb repulsion U , in agreement with experimental observation of a metallic state in SrVO_3 .

In the early transition metal oxides, we projected the Kohn-Sham solution to the t_{2g} states, because the center of the eg states is sufficiently above the Fermi level that it does not require dynamic treatment within the DMFT. Since the eg states strongly hybridize with the oxygen, the eg occupancy does not exactly vanish. However, the DFT+DMFT solution is very sensitive to the correlated t_{2g} occupancy in early transition metal oxides, since the eg states behave very differently, having a large gap. Hence, the eg and t_{2g} charge should not be counted together when assessing stability of the DMFT insulating solution, hence we presented the t_{2g} charge only in tables I,II.

V. CONCLUSIONS

We have shown in this paper that with the DFT+DMFT methodology of Ref. 43, a reasonable qualitative agreement between theory and experiment for the p and d spectra across the transition metal series is obtained, even when the Coulomb repulsion U and J are fixed across the entire series, hence no tuning parameter is needed for qualitative description of correlated solids, which is a requirement for any ab-initio predictive method. This was possible because the DFT+DMFT method is implemented with a very localized projector, where the screening of the Coulomb repulsion by other valence states through hybridization is very efficient.

A large effort was undertaken recently by several groups^{43–48} to implement DFT+DMFT in a way that does not require tuning parameters, and that has *ab initio* predictive power. In our opinion, such mature state of DFT+DMFT has largely been reached, as demonstrated on early and late transition metal oxides here. This method gives a zeroth-order picture of the physics in correlated materials such as transition metal oxides. However, the position of oxygen states is not very precise in some compounds (see LaTiO₃), and better treatment of exchange would be needed to mitigate this deficiency. It was recently proposed in Ref.91 that additional Hartree term due to non-local interaction U_{pd} could mitigate this problem. However, in the charge-self-consistent DFT+DMFT used here, the Hartree terms are taken into account exactly, and therefore no extra Hartree shifts are justified. Further corrections could come only from better treatment of the non-local exchange. Furthermore, the gap sizes of Mott insulators and positions of Hubbard bands can be improved by calculating Coulomb U more precisely from first principles. This is an important open problem in condensed matter theory. Methods such as GW⁹² and constrained-RPA⁹³ show some promise in this direction, but more work is needed to get precise enough values of U for modern DFT+DMFT codes, which use localized atomic orbitals in a large energy window.

In our implementation of DFT+DMFT, the position of oxygen states is not very far from its DFT value, and quite insensitive to the value of the correlation strength, in contrast to finding of Refs. 50,51. While the position of the oxygen states in DFT are not always in very good agreement with experiment, their small displacement does not lead to a major failure of DFT+DMFT. This shortcoming of LDA is known to occur in other materials (see for example Ref. 90) and can be corrected by a better treatment of the non-local exchange as in hybrid DFT or GW, but not by DMFT.

We have also shown in this paper that in transition metal oxides the self-consistent value of the correlated electronic charge n_d of LDA+DMFT is closer to nominal valence than its LDA value. A similar finding was reported in Ref. 54 when studying the actinide series and its compounds. A systematic comparison with the X-ray data confirmed that the LDA+DMFT systematically improves the value of the correlated charge, n_f , relative to its LDA value.

Finally, the DMFT method is an orbitally dependent method, and the results depend on the choice of the correlated set of orbitals. The convergence of the results with respect to the number of orbitals is not possible at present, because the quantum mechanical problem becomes too expensive to solve. The quality of the results hence rest on the educated choice of the correlated orbital (the choice of the projector) which determines the set of states that are treated very precisely, by summing all local Feynman diagrams, and those that are treated by DFT. Since DMFT truncates interaction and correlations beyond single site, a more localized orbital is clearly a better choice in this method. To recover similar results in a more delocalized basis, one would clearly need to go beyond single site approximation, which increases computational expense exponentially.

We have shown that in transition metal oxides, the $3d$ occupancies (n_d) on the transition metal ion are not very far from nominal valence when sufficiently localized radial function is chosen for the projector. This is true even on the DFT level. We have also explicitly demonstrated that the choice of a more delocalized radial orbital leads to valences substantially larger than the nominal valence, which poses a problem for DMFT method, as noted in Refs. 50,51. For such a choice of correlated states, the non-local correlations would likely need to be considered to recover similar results as in more localized case.

In conclusion, we successfully tested our implementation of the DFT+DMFT method in $3d$ transition metal series. The method predicts qualitative features, such as existence of a metallic or insulating state starting from first principles. It can be made fully automated, and hence high-throughput screening of correlated materials is an attractive avenue for future research.

VI. ACKNOWLEDGMENTS

We thank A. Georges, C. H. Yee, H. Park, and A. J. Millis for stimulating discussion. KH, GK were supported by NSF DMR–1405303, and NSF DMR–1308141, respectively.

* Electronic address: haule@physics.rutgers.edu

¹ H. Bethe, Ann. Phys. (Leipzig) **392**, 55 (1928).

² A. Sommerfeld, Z. Elektrochem. Angew. Phys. Chem. **34**,

426 (1928).

³ F. Bloch, Z. Phys. **57**, 545 (1929).

⁴ A. A. Abrikosov, L. P. Gor'kov, and I. Ye. Dzyaloshinskii,

- Quantum Field Theoretical Methods in Statistical Physics*, 2nd ed. (Pergamon, Oxford, 1965).
- ⁵ N. F. Mott, Proc. Phys. Soc. London **49** (Part 1), 72 (1937)
 - ⁶ N. F. Mott, Metal-Insulator Transitions. 2nd ed. Taylor
 - ⁷ N. F. Mott and R. Peierls, Proc. Phys. Soc. **49**, A72 (1937). & Francis: London. 1990 <http://badmetals.magnet.fsu.edu/pdfs/Mott90book-chap8.pdf>
 - ⁸ M. Imada, A. Fujimori, and Y. Tokura, Rev. Mod. Phys. **70**, 1039 (1998).
 - ⁹ D.N. Basov, Richard D. Averitt, Dirk van der Marel Martin Dressel, Kristjan Haule, Rev. Mod. Phys. **83**, 471 (2011).
 - ¹⁰ P. Hohenberg, and W. Kohn, Phys. Rev. **136**, B864B871 (1964).
 - ¹¹ A. Georges, and G. Kotliar, Phys. Rev. B **45**, 6479 (1992).
 - ¹² W. Metzner and D. Vollhardt, Phys. Rev. Lett. **62**, 324 (1989).
 - ¹³ A. Georges, G. Kotliar, W. Krauth, and M. J. Rozenberg, Rev. Mod. Phys. **68**, 13 (1996).
 - ¹⁴ G. Kotliar, and D. Vollhardt, Phys. Today **57** (3), 53 (2004).
 - ¹⁵ X. Y. Zhang, M. J. Rozenberg, and G. Kotliar, Phys. Rev. Lett. **70**, 1666 (1993).
 - ¹⁶ M. J. Rozenberg, G. Kotliar, and X. Y. Zhang, Phys. Rev. B **49**, 10181 (1994).
 - ¹⁷ A. Georges and W. Krauth, Phys. Rev. Lett. **69**, 1240 (1992).
 - ¹⁸ M. J. Rozenberg, G. Kotliar, H. Kajueter, G. A. Thomas, D. H. Rapkine, J. M. Honig and P. Metcalf, Phys. Rev. Lett. **75**, 105 (1995).
 - ¹⁹ P. Limelette, A. Georges, D. Jerome, P. Wzietek, P. Metcalf, and J. M. Honig, Science **302**, 89 (2003).
 - ²⁰ P. Semon and A.-M. S. Tremblay, Phys. Rev. B **85**, 201101(R) (2012).
 - ²¹ Anisimov, Poteryaev, Korotin, Anokhin, Kotliar J. Phys.: Condens. Matter **9**, 7359 (1997); Lichtenstein, Katsnelson Phys. Rev. B **57**, 6884 (1998)
 - ²² G. Kotliar, S. Y. Savrasov, K. Haue, V. S. Oudovenko, O. Parcollet, and C. A. Marianetti, Rev. Mod. Phys. **78**, 865 (2006).
 - ²³ K. Held, Advances in Physics **56**, 829 (2007).
 - ²⁴ S. Savrasov, G. Kotliar, and E. Abrahams, Nature (London) **410**, 793 (2001).
 - ²⁵ X. Dai, S. Y. Savrasov, G. Kotliar, A. Migliori, H. Ledbetter, and E. Abrahams, Science **300**, 953 (2003).
 - ²⁶ J.H. Shim, K. Haule, G. Kotliar, Science **2007**, 1615 (2007).
 - ²⁷ M.B Zolfl, I.A. Nekrasov, Th. Pruschke, V.I. Anisimov, J. Keller, Phys. Rev. Lett. **87**, 276403 (2001).
 - ²⁸ K. Held, A.K. McMahan, R.T. Scalettar, Phys. Rev. Lett. **87**, 276404 (2001).
 - ²⁹ E.R. Ylvisaker, J. Kunes, A.K. McMahan, W.E. Pickett, Phys. Rev. Lett. **102**, 246401 (2009).
 - ³⁰ B. Amadon, S. Biermann, A. Georges, and F. Aryasetiawan, Phys. Rev. Lett. **96**, 066402 (2006).
 - ³¹ E. Pavarini, S. Biermann, A. Poteryaev, A.I. Lichtenstein, A. Georges, O.K. Andersen, Phys. Rev. Lett. **92**, 176403 (2004).
 - ³² E. Pavarini, A. Yamasaki, J. Nuss, O. K. Andersen, New J. Phys. **7**, 188 (2005).
 - ³³ M. De Raychaudhury, E. Pavarini, and O. K. Andersen, Phys. Rev. Lett. **99**, 126402 (2007).
 - ³⁴ I.A. Nekrasov, G. Keller, D.E. Kondakov, A.V. Kozhevnikov, Th. Pruschke, K. Held, D. Vollhardt, V.I. Anisimov, Phys. Rev. B **72**, 155106 (2005).
 - ³⁵ K. Ohta, R.E. Cohen, K. Hirose, K. Haule, K. Shimizu, Y. Ohishi, Phys. Rev. Lett. **108**, 026403 (2012).
 - ³⁶ E. Gorelov, M. Karolak, T.O. Wehling, F. Lechermann, A.I. Lichtenstein, E. Pavarini, Phys. Rev. Lett. **104**, 226401 (2010).
 - ³⁷ J. Mravlje, M. Aichhorn, T. Miyake, K. Haule, G. Kotliar, and A. Georges, Phys. Rev. Lett. **106**, 096401 (2011).
 - ³⁸ H. Zhang, K. Haule, D. Vanderbilt, arXiv:1308.4471.
 - ³⁹ G.H. Wannier, Phys. Rev. **52**, 191 (1937).
 - ⁴⁰ F. Aryasetiawan, M. Imada, A. Georges, G. Kotliar, S. Biermann, and A. I. Lichtenstein, Phys. Rev. B **70**, 195104 (2004).
 - ⁴¹ T. Miyake, F. Aryasetiawan, and M. Imada, Phys. Rev. B **80**, 155134 (2009).
 - ⁴² S. Y. Savrasov and G. Kotliar, Phys. Rev. B **69**, 245101 (2004).
 - ⁴³ K. Haule, C.-H. Yee, and K. Kim, Phys. Rev. B **81**, 195107 (2010).
 - ⁴⁴ B. Amadon, F. Lechermann, A. Georges, F. Jollet, T. O. Wehling, and A. I. Lichtenstein, Phys. Rev. B **77**, 205112 (2008).
 - ⁴⁵ B. Amadon, J. Phys.: Condens. Matter **24** 075604 (2012).
 - ⁴⁶ F. Lechermann, A. Georges, A. Poteryaev, S. Biermann, M. Posternak, A. Yamasaki, and O. K. Andersen, Phys. Rev. B **74**, 125120 (2006).
 - ⁴⁷ O. Granas, I. Di Marco, P. Thunstrom, L. Nordstrom, O. Eriksson, T. Bjorkman, and J. M. Wills, Computational Materials Science **55**, 295 (2012).
 - ⁴⁸ M. Aichhorn, L. Pourovskii, and A. Georges, Phys. Rev. B **84**, 054529 (2011).
 - ⁴⁹ N. Marzari, A.A. Mostofi, J.R. Yates, I. Souza, and D. Vanderbilt, Rev. Mod. Phys. **84**, 1419 (2012).
 - ⁵⁰ X. Wang, M. J. Han, L. de Medici, H. Park, C. A. Marianetti, and A. J. Millis, Phys. Rev. B **86**, 195136 (2012).
 - ⁵¹ Hung T. Dang, Andrew J. Millis, and Chris A. Marianetti, Phys. Rev. B **89**, 161113(R) (2014).
 - ⁵² J. H. Shim, K. Haule, and G. Kotliar, Nature **446**, 513-516 (2007).
 - ⁵³ J. H. Shim, K. Haule, S. Savrasov, G. Kotliar, Phys. Rev. Lett. **101**, 126403 (2008).
 - ⁵⁴ J. H. Shim, K. Haule and G. Kotliar, Eur. Phys. Lett. **85**, 17007 (2009).
 - ⁵⁵ K. Haule and G. Kotliar, Nature Physics **5**, 796 - 799 (2009).
 - ⁵⁶ Chuck-Hou Yee, G. Kotliar, and K. Haule, Phys. Rev. B **81**, 035105 (2010).
 - ⁵⁷ M. K. Stewart, J. Liu, R. K. Smith, B. C. Chapler, C.-H. Yee, K. Haule, J. Chakhalian, D. N. Basov, J. Appl. Phys. **110**, 033514 (2011).
 - ⁵⁸ Z. P. Yin, K. Haule, G. Kotliar, Nature Physics **7**, 294 (2011).
 - ⁵⁹ M. E. Pezzoli, K. Haule, and G. Kotliar, Phys. Rev. Lett. **106**, 016403 (2011).
 - ⁶⁰ M. K. Stewart, C.-H. Yee, J. Liu, M. Kareev, R. K. Smith, B. C. Chapler, M. Varela, P. J. Ryan, K. Haule, J. Chakhalian, and D. N. Basov, Phys. Rev. B **83**, 075125 (2011).
 - ⁶¹ Q. Yin, A. Kutepov, K. Haule, G. Kotliar, S. Y. Savrasov, W. E. Pickett, Phys. Rev. B **84**, 195111 (2011).
 - ⁶² Z. P. Yin, K. Haule, G. Kotliar, Nature Materials **10**, 932-935 (2011).
 - ⁶³ J.-X. Zhu, P. H. Tobash, E. D. Bauer, F. Ronning, B. L. Scott, K. Haule, G. Kotliar, R. C. Albers, J. M. Wills,

- Eur. Phys. Lett. **97**, 57001 (2012).
- ⁶⁴ K. Ohta, R. E. Cohen, K. Hirose, K. Haule, K. Shimizu, Y. Ohishi, Phys. Rev. Lett. **108**, 026403 (2012).
- ⁶⁵ X. Deng, K. Haule, G. Kotliar, arXiv:1308.2245
- ⁶⁶ M. Liu, L. W. Harriger, H. Luo, M. Wang, R. A. Ewings, T. Guidi, H. Park, K. Haule, G. Kotliar, S. M. Hayden, and P. Dai, Nature Physics **8**, 376 (2012).
- ⁶⁷ J. M. Tomczak, K. Haule, and G. Kotliar, Proc. Natl. Acad. Sci. USA **109** 3243 (2012).
- ⁶⁸ H. C. Choi, B. I. Min, J. H. Shim, K. Haule, G. Kotliar, Phys. Rev. Lett. **108**, 016402 (2012).
- ⁶⁹ G. Lee, H. S. Ji, Y. Kim, C. Kim, K. Haule, G. Kotliar, B. Lee, S. Khim, K. H. Kim, K. S. Kim, K.S. Kim, and J. H. Shim, Phys. Rev. Lett. **109**, 177001 (2012).
- ⁷⁰ H. C. Choi, K. Haule, G. Kotliar, B. I. Min, and J. H. Shim, Phys. Rev. B **88**, 125111 (2013).
- ⁷¹ K. Haule, *Phys. Rev. B* **75**, 155113 (2007).
- ⁷² P. Werner, A. Comanac, L. de Medici, M. Troyer, and A. J. Millis, *Phys. Rev. Lett.* **97**, 076405 (2006).
- ⁷³ V. I. Anisimov, F. Aryasetiawan, and A. I. Lichtenstein, J. Phys.: Condens. Matter **9**, 767 (1997).
- ⁷⁴ P. Blaha, K. Schwarz, G. K. H. Madsen, K. Kvasnicka, and J. Luitz, in Wien2K, edited by K. Schwarz (Technische Universitat Wien), Austria, 2001.
- ⁷⁵ J.P. Perdew, K. Burke, and M. Ernzerhof, Phys. Rev. Lett. **77**, 3865 (1996).
- ⁷⁶ M. J. Rey, Ph. Dehaudt, J. C. Joubert, B. Lambert-Andron, M. Cyrot and F. Cyrot-Lackmann, Journal of Solid State Chemistry **86**, 101 (1990).
- ⁷⁷ P. Bordet, C. Chaillout, M. Marezio, Q. Huang, A. Santoro, S.-W. Cheong, H. Takagi, C. S. Oglesby, B. Batlogg, Journal of Solid State Chemistry **106**, 253 (1993).
- ⁷⁸ D.A. MacLean, H. H. Ng, J. E. Greedan, Journal of Solid State Chemistry (1979) **30**, 35 (1979).
- ⁷⁹ T. Kajitani, K. Hiraga, T. Sakurai, M. Hirabayashi, S. Hosoya, T. Fukuda and K. Oh-Ishi, Physica C: Superconductivity **171**, 491 (1990).
- ⁸⁰ M. Jarrell, and J. E. Gubernatis, Physics Reports **269**, 133 (1996).
- ⁸¹ K. Momma, and F. Izumi, J. Appl. Crystallogr. **44**, 1272 (2011).
- ⁸² K. Yoshimatsu, T. Okabe, H. Kumigashira, S. Okamoto, S. Aizaki, A. Fujimori, and M. Oshima, Phys. Rev. Lett. **104** 147601 (2010).
- ⁸³ K. Maiti and D. D. Sarma, Phys. Rev. B **61**, 2525 (2000).
- ⁸⁴ T. Yoshida, A. Ino, T. Mizokawa, A. Fujimori, Y. Taguchi, T. Katsufuji and Y. Tokura, Europhys. Lett. **59**, 258 (2002).
- ⁸⁵ T. Takahashi, F. Maeda, H. Katayama-Yoshida, Y. Okabe, and T. Suzuki, A. Fujimori, S. Hosoya, S. Shamoto and M. Sato, Phys. Rev. B **37**, 9788 (1988).
- ⁸⁶ T. Yoshida, K. Tanaka, H. Yagi, A. Ino, H. Eisaki, A. Fujimori, and Z.-X. Shen, Phys. Rev. Lett. **95**, 146404 (2005).
- ⁸⁷ P.M. Woodward, Acta Crystallogr. Sect. A. **53**, 44 (1997).
- ⁸⁸ M. Cwik, T. Lorenz, J. Baier, R. Muller, G. Andre, F. Bouree, F. Lichtenberg, A. Freimuth, R. Schmitz, E. Muller-Hartmann, and M. Braden, Phys. Rev. B **68**, 060401(R) (2003).
- ⁸⁹ V. S. Oudovenko, G. Palsson, S. Y. Savrasov, K. Haule, and G. Kotliar, Phys. Rev. B **70**, 125112 (2004).
- ⁹⁰ Z. P. Yin, A. Kutepov, and G. Kotliar, Phys. Rev. X **3**, 021011 (2013).
- ⁹¹ P. Hansmann, N. Parragh, A. Toschi, G. Sangiovanni, and K. Held, arXiv:1312.2757.
- ⁹² A. Kutepov, K. Haule, S.Y. Savrasov, G. Kotliar, Phys. Rev. B **82**, 045105 (2010).
- ⁹³ F. Aryasetiawan, M. Imada, A. Georges, G. Kotliar, S. Biermann, and A. I. Lichtenstein, Phys. Rev. B **70**, 195104 (2004).
- ⁹⁴ M. Takizawa, M. Minohara, H. Kumigashira, D. Toyota, M. Oshima, H. Wadati, T. Yoshida, A. Fujimori, M. Lippmaa, M. Kawasaki, H. Koinuma, G. Sordi, and M. Rozenberg, Phys. Rev. B **80**, 235104 (2009).
- ⁹⁵ G. Sordi, A. Amaricci, and M. J. Rozenberg, Phys. Rev. Lett. **99**, 196403 (2007).
- ⁹⁶ Juho Lee and Kristjan Haule, arXiv:1403.2474v1.